IEEE Access
Multidisciplinary ⋮ Rapid Review ⋮ Open Access Journal

Received 8 December 2023, accepted 8 January 2024, date of publication 16 January 2024,
date of current version 25 January 2024.

Digital Object Identifier 10.1109/ACCESS.2024.3354983

RESEARCH ARTICLE

Research on Cooling Problem of a Modular Permanent Magnet Synchronous Machine Based on a 3D Equivalent Thermal Network Method

YINGYING XU[1], TIANTIAN LIANG[1], MINGXIA XU[1], CHUANFANG XU[1], QINGGUANG CHI[1], AND HAIYU LIU[2]

[1]School of Automation and Electrical Engineering, Dalian Jiaotong University, Dalian 116028, China
[2]CRRC Dalian Company Ltd., Dalian 116045, China

Corresponding author: Yingying Xu (xuyingying7520@163.com)

This work was supported in part by the Science and Technology Bureau of Dalian, Liaoning, China, under Grant 2023RQ061.

ABSTRACT Due to the huge volume of gearless ball mill direct drive permanent magnet synchronous machine (PMSM), an unwinding modular technology is convenient for its redundant power control, manufacture and maintenance. Several module units are wrapped around the ball mill roller for direct drive. The motor frame adopts a modular structure to achieve complete decoupling between modules. And the cooling problem of the motor is very important for its stable operation. The traditional waterway structure design and cooling analysis methods are difficult to meet the engineering requirements of large modular permanent magnet synchronous machine (MPMSM). A 3D equivalent thermal network method is proposed to study the cooling problem of MPMSM. The design program of modular frame cooling structure is written based on a 3D equivalent thermal network method. According to the temperature distribution of each node, the cyclic check is carried out to quickly design the modular waterway. The cooling effect of the designed waterway structure is analyzed by fluid-solid coupled temperature field simulation. An 80 kW prototype is developed and the temperature rise experiment is carried out. The simulation and experiment results prove the rationality of a 3D equivalent thermal network method for the MPMSM cooling structure design.

INDEX TERMS MPMSM, module decoupling, modular frame cooling structure, 3D equivalent thermal network, fluid-solid coupled temperature field.

I. INTRODUCTION

With the large-scale development of ball mills, a direct drive gearless ball mill appears, which eliminates the limitation of transmission torque of large gears. However, it is difficult to process, transport, install and maintain the gearless ball mill because of its huge volume and coils can not be decoupled freely. The appearance of modular technology has solved a series of problems caused by large volume of the motor [1], [2]. This paper presents a modular permanent magnet synchronous machine (MPMSM) with wrapped type for mine ball mill. The motor is modularized by removing part of coils, and each module can run independently. It is convenient for redundant power control, manufacture and maintenance of the motor. Its frame also adopts a modular structure to achieve complete decoupling between modules. In order to ensure the stable operation of MPMSM, it is necessary to study its cooling problem.

Recently the analysis of cooling problems and the calculation of temperature rises have become research hotspots in the field of motors. Fan et al. [3] proposed an advanced cooling configuration of several water cold plates radially inserted into the core laminations of PMSM. Li and Zhu [4] used grease buffers filled between stator cores and

The associate editor coordinating the review of this manuscript and approving it for publication was Wen-Sheng Zhao.

motor housings to improve the electromagnetic, thermal, and stress-deformation performances of PMSM. Zhu et al. [5] proposed a double-circulatory technique in conjunction with a two-way coupling of physical parameters to determine the motor temperature distribution. Vansompel and Sergeant [6] introduced a thermally conductive insert piece that encloses the stator end-windings with extensions in the stator slots to increase the heat conduction between the stator windings and the housing. Although the above structure has a good cooling effect, the traditional water jacket with axial or circumferential ducts is still the most used type of liquid forced convection because of its effectiveness and manufacturability [7], [8], [9].

Yu et al. [10], [11] adopted the lumped-parameter thermal model combined with the finite element method to study the steady-state temperature distribution and transient-state temperature rise of PMSM. The thermal network method is short in calculation time, but its calculation accuracy depends on the rationality of the thermal network model. He et al. [12], [13] used the fluid-solid coupled simulation to analyze the influence of different cooling methods, flow rate and coolant on the thermal design of the motor. Most motors use the finite element method to calculate the overall temperature [14], [15], [16]. However, its solution time is too long for large motors, which is difficult to their early designs.

To sum up, a 3D equivalent thermal network method is proposed to study the cooling problem of MPMSM. According to the temperature distribution of the radial and axial nodes, the cyclic check is carried out to quickly design a reasonable modular waterway structure. The cooling effect of the designed waterway structure is analyzed by the fluid-solid coupled temperature field simulation. An 80 kW prototype is developed. The correctness of the designed modular waterway structure based on a 3D equivalent thermal network method is verified through experiments, which provides a reference for the research on the cooling problem of MPMSM.

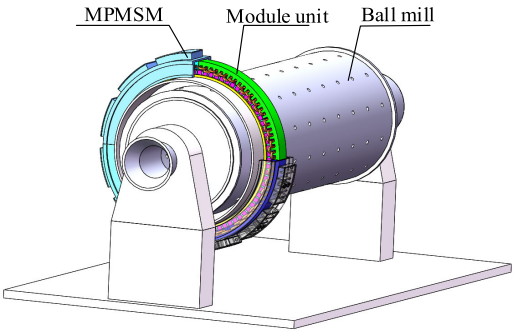

FIGURE 1. MPMSM direct drive mode.

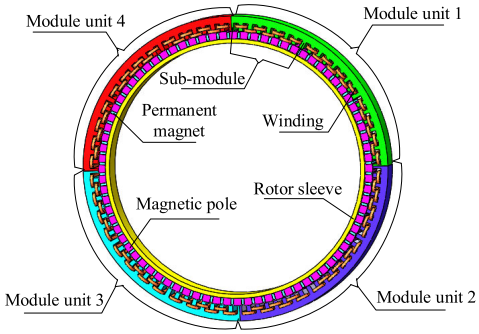

FIGURE 2. Internal tructure of MPMSM.

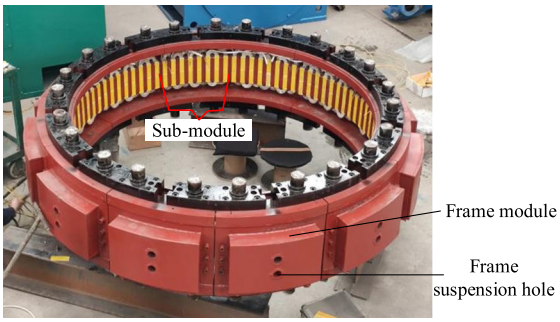

FIGURE 3. Moduar frame and stator of MPMSM.

II. MPMSM STRUCTURE

The model of a direct drive MPMSM for ball mills is shown in Fig. 1. The MPMSM is wrapped around the ball mill roller to realize the direct drive without gears, which greatly improves the reliability and transmission efficiency. The motor adopts an unwinding modular technology, removing part of coils on the stator teeth, and parting blocks in the blank teeth. The internal structure of MPMSM is shown in Fig. 2, which designed in this paper consists of 4 module units. A sub-module is from one unwinding stator slot to the next one. A module unit is composed of several sub-modules [17]. Each module unit can be regarded as a small independent rotary motor. It is convenient for manufacture, maintenance, fault-tolerant operation and redundant power control of large motors.

In order to achieve complete decoupling between modules, the frame also adopts the modular structure. The water-cooled frame modules and motor stator are shown in Fig. 3. A sub-module is attached to a frame module. There is no waterway in the contact part between the frame modules, and the waterway accounts for 3/4 of the whole frame module. The waterways between the frame modules are connected in series through pipes.

Although there is no span winding between the adjacent sub-modules, it has an installation air gap and there is no waterway in the upper frame module. Therefore, the calculation of the radial temperature of MPMSM can not be ignored. The traditional water structure design and cooling analysis methods are difficult to meet the engineering requirements of large MPMSM. It is very important to find a simple and fast method to calculate temperature rise for the initial design of the MPMSM modular cooling structure.

III. 3D EQUIVALENT THERMAL NETWORK CALCULATION

A. 3D EQUIVALENT THERMAL NETWORK MODEL

The frame adopts the axial series modular waterway structure. The design program of modular frame cooling structure is written based on the waterway thermodynamic calculation and 3D equivalent thermal network method.

According to the temperature distribution of each node, the cyclic check is carried out to quickly design a modular waterway, so that MPMSM can run stably under the limiting condition of temperature rise. The 3D equivalent thermal network model of MPMSM is established, as shown in Fig. 4. The waterway structure of each sub-module is symmetrical along the circumferential direction. Therefore, the radial thermal network model is simplified into a sub-module radial thermal network model.

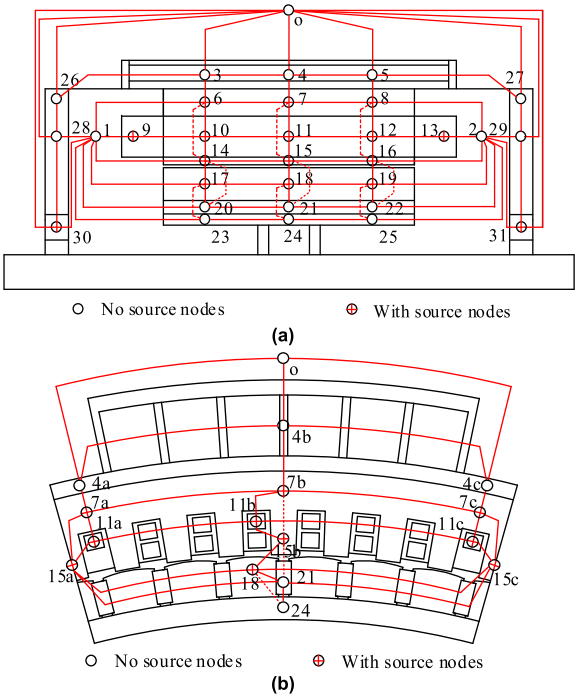

FIGURE 4. 3D Equivalent thermal network model of MPMSM: (a) axial structure; (b) radial structure of a sub-module.

Fig. 4(a) is the MPMSM axial network model, in which the part represented by each node and the heat source distribution are the same as those in reference [18]. Fig. 4(b) is the radial thermal network model of a sub-module at the axial center section of the motor. o represents an ambient temperature node; 4a-4c represent water-cooled frame nodes; 7a-7c represent stator yoke nodes; 11a-11c represent winding nodes; 15a-15c represent stator tooth nodes; 18 represent rotor magnetic pole node; 21 represents permanent magnet node; 24 represents rotor sleeve node.

The heat sources in a sub-module are distributed as follows. The stator core loss of a sub-module is equably distributed over nodes 7a-7c and 15a-15c; the copper loss of a sub-module is equably distributed over nodes 11a-11c; the stray loss of a sub-module is equably distributed over nodes 15a-15c and 18.

B. RADIAL THERMAL NETWORK PARAMETERS

The calculation of thermal resistance in the axial structure and rotor part in radial structure is similar to that of reference [18], and it will not be described. The thermal resistance of the stator and frame in the radial structure of MPMSM is calculated as follows.

1) THERMAL RESISTANCE OF FRAME MODULE

We take the water-cooled frame node 4b as an example. Heat transfer is divided into three paths. These paths correspond to the temperature boundary, the same layer nodes in the radial direction and the stator yoke. A frame module parameters are shown in Fig. 5.

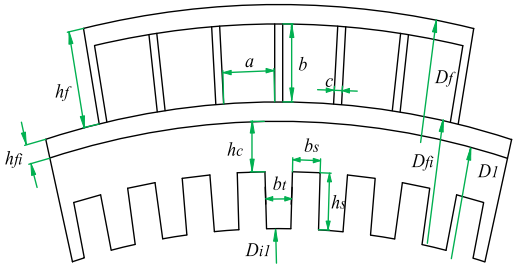

FIGURE 5. Parameters of frame module: D_f-outer diameter of frame with waterway part, D_{fi}-outer diameter of frame without waterway part, D_1-outer diameter of stator, D_{i1}-internal diameter of stator, h_f-thickness of frame with waterway part, h_{fi}-thickness of frame without waterway part, h_c-thickness of stator core yoke, b_t-width of stator tooth, b_s-width of stator slot, h_s-height of stator slot, a-width of cooling channel, b-height of cooling channel, and c-thickness of baffle plate.

The thermal resistance between nodes 4b and o can be expressed as follows:

$$R_{4bo} = \frac{h_f/2}{\lambda_f S_{4bo\lambda}} + \frac{1}{\alpha_f S_{4boc}} \tag{1}$$

$$S_{4bo\lambda} = \pi D_f L_f/48 \tag{2}$$

$$S_{4boc} = CL_f/36 \tag{3}$$

where L_f is the axial length of the frame; C is the wet perimeter of the water channel; λ_f is the heat conductivity coefficient of the water-cooled frame; α_f is the channel heat dissipation coefficient; $S_{4bo\lambda}$ is the radial heat conduction area of the frame; S_{4boc} is the convective heat dissipation area between the water and the frame.

The thermal resistance between nodes 4b and 4a can be expressed as:

$$R_{4b4a} = \frac{\pi D_{fi}/24}{\lambda_f S_{4b4a}} \tag{4}$$

$$S_{4b4a} = h_{fi} L_f/3 \tag{5}$$

where S_{4b4a} is the heat conduction area of the end and middle part of the frame module.

The heat is transferred from node 7b to node 4b through an assembly gap between the stator and the frame. The thermal

resistance between nodes $4b$ and $7b$ can be expressed as:

$$R_{4b7b} = \frac{h_c/2}{\lambda_c S_{4b7bc}} + \frac{L_{4b7b}}{\lambda_a S_{4b7b}} + \frac{h_f/2}{\lambda_f S_{4b7b}} \tag{6}$$

$$S_{4b7bc} = \pi\left(D_1 - h_c/2\right)L/48 \tag{7}$$

$$S_{4b7b} = \pi D_1 L/48 \tag{8}$$

$$L_{4b7b} = (3D_1 + 0.5) \times 10^{-5} \tag{9}$$

where L is the axial length of the stator; λ_c is the radial heat conductivity coefficient of the silicon steel sheet; λ_a is the heat conductivity coefficient of air; L_{4b7b} is the mounting clearance between the stator and the frame; S_{4b7bc} is the average heat dissipation area of the stator yoke; and S_{4b7b} is the heat dissipation area between the frame and the stator.

2) THERMAL RESISTANCE OF STATOR YOKE

We take the stator yoke node $7b$ as an example. Heat transfer is divided into four paths. These paths correspond to the frame module, the same layer nodes in the radial direction, the winding, and the stator tooth. The thermal resistance between nodes $7b$ and $7a$ can be expressed as:

$$R_{7b7a} = \frac{\pi\left(D_1 - h_c\right)/24}{\lambda_c h_c L/3} \tag{10}$$

The thermal resistance between nodes $7b$ and $11b$ can be expressed as [19]:

$$R_{7b11b} = \frac{1}{k_s S_{7b11b}} \tag{11}$$

$$S_{7b11b} = 6b_s L/3 \tag{12}$$

$$\frac{1}{k_s} = \frac{\delta_i}{\lambda_i} + \frac{1}{4}\left[\frac{b_s(1-\sqrt{s_f})}{\lambda_L}k_L + \frac{b_s(1-\sqrt{s_f})}{\lambda_{oil}}(1-k_L) + \frac{\delta_d b_s\sqrt{s_f}}{d\lambda_d}\right] \tag{13}$$

where S_{7b11b} is the heat dissipation area between the stator yoke and the winding; k_s is the equivalent heat conductivity coefficient of the winding in the stator slot; δ_i is the insulation thickness of the slot; λ_i is the heat conductivity coefficient of the slot insulation; s_f is slot full rate; λ_L is the heat conductivity of the impregnated paint; k_L is the paint filling coefficient; λ_{oil} is the heat conductivity coefficient of stationary oil layer; δ_d is the thickness of enameled wire; λ_d is the heat conductivity coefficient of the wire paint layer; d is the outside diameter of bare copper wire.

The thermal resistance between nodes $7b$ and $15b$ can be expressed as:

$$S_{7b15bc} = \pi\left(D_1 - h_c\right)L/48 \tag{14}$$

$$S_{7b15bt} = 6b_t L/3 \tag{15}$$

$$R_{7b15b} = \frac{h_c/2}{\lambda_c S_{7b15bc}} + \frac{h_s/2}{\lambda_c S_{7b15bt}} \tag{16}$$

where S_{7b15bc} is the heat dissipation area of the stator yoke; S_{7b15bt} is the heat dissipation area of the stator tooth.

3) THERMAL RESISTANCE OF WINDING

We take the winding node $11b$ as an example. Heat transfer is divided into three paths. These paths correspond to the stator yoke, the same layer nodes in the radial direction and the stator tooth. The thermal resistance between nodes $11b$ and $11a$ can be expressed as:

$$R_{11b11a} = \frac{\pi\left(D_{i1} + h_s\right)/32}{\lambda_{cu} bL/3} \tag{17}$$

where λ_{cu} is the heat conductivity coefficient of copper.

The thermal resistance between nodes $11b$ and $15b$ can be expressed as:

$$R_{11b15b} = \frac{1}{4h_s L k_s} \tag{18}$$

4) THERMAL RESISTANCE OF STATOR TOOTH

We take the stator tooth node $15b$ as an example. Heat transfer is divided into four paths. These paths correspond to the winding, the stator yoke, the rotor pole and the rotor permanent magnet. The thermal resistance between nodes $15b$, 18, and 21 can be expressed as [20]:

$$R_{15bg} = \frac{h_s/2}{\lambda_c 6b_t L/3} + \frac{1}{\alpha_g 6b_t L/3} \tag{19}$$

where α_g is the air gap heat dissipation coefficient between stator and rotor.

C. HEAT BALANCE EQUATION

According to the principle of heat balance, for the 43 nodes of the whole motor, the heat balance equations need to be listed. The matrix form of heat balance equation can be written as:

$$GT = W \tag{20}$$

where G is the heat conductance matrix of order 43; T is the temperature rise matrix; W is the heat source loss matrix.

D. MODULAR WATERWAY STRUCTURE DESIGN

The initial parameters of modular waterway structure are determined according to the waterway thermodynamic calculation. Then a 3D equivalent thermal network model is established according to the waterway parameters. Based on the results of 3D equivalent thermal network calculation, the waterway structure is constantly modified to form a design program of modular waterway structure.

The flow chart for the modular waterway design of MPMSM is shown in Fig. 6. When the calculation result of temperature meets the temperature rise requirement of MPMSM, the cycle is finished. The modular waterway structure is determined.

The node temperature of an 80 kW MPMSM solved by a 3D equivalent thermal network method is shown in Table 1. In the axial node temperature, the average temperature of the winding is 79.6 °C, which meets the temperature rise requirements of class F insulation. In the radial node temperature of a sub-module, the temperature of the part without waterway is lower than the part with waterway. A coil is

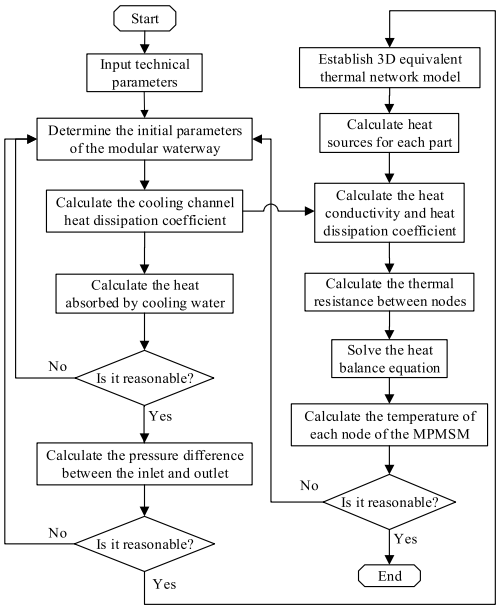

FIGURE 6. Flow chart for modular waterway design.

TABLE 1. Calculated node temperature.

Components	Axial node temperature/°C				
Frame		3/30.2	4/30.06	5/30.2	
Stator yoke		6/47.9	7/47.2	8/47.9	
Winding	9/80.4	10/79.3	11/78.8	12/79.3	13/80.4
Stator tooth		14/55.8	15/55.1	16/55.8	
Magnetic pole		17/79.5	18/79.2	19/79.5	
Magnet		20/80.9	21/80.7	22/80.9	
Rotor sleeve		23/71.4	24/71.8	25/71.4	
Front cover		26/30.7		28/45.2	
Rear cover		27/30.7		29/45.2	
Bearing		30/58.0		31/58.0	
Chamber air		1/64.3		2/64.3	
Surroundings			o/27.4		
Components	Radial node temperature of a sub-module/°C				
Frame	4a/36.7		4b/30.1		4c/36.7
Stator yoke	7a/47.2		7b/47.1		7c/47.2
Winding	11a/78.5		11b/78.8		11c/78.5
Stator tooth	15a/55.9		15b/55.3		15c/55.9

TABLE 2. Design parameters of the modular waterway structure.

Items	Value
Number of channels	72
Cooling channel height (mm)	80
Cooling channel width (mm)	60
Baffle plate thickness (mm)	10
Axial length of channel (mm)	225

removed there, and the heat generated by the copper loss of the winding is half of the original, so its temperature is lower. The highest temperature of the winding in the radial nodes is 78.8 °C, which does not exceed the temperature limit, and the temperature cycle ends. Therefore, the MPMSM adopts this axial series modular waterway structure in Table 2.

IV. FLUID-SOLID COUPLED SIMULATION

In order to reduce the calculation time, the solution domain physical model of a module is established for the 80 kW MPMSM with above modular waterway structure, as shown in Fig. 7. Since the motor is composed of four identical and decoupled module units, the temperature field of one module unit can be solved.

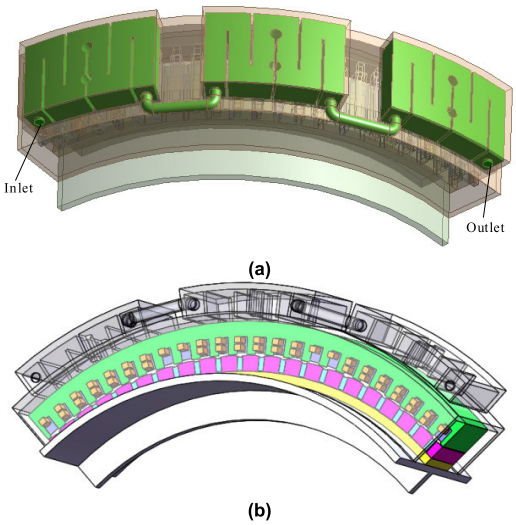

FIGURE 7. Physical model in solution region: (a) modular waterway; (b) one sub-module.

The initial temperature of the simulation model is set to 300 K. Fluent software is used to simulate the fluid-solid coupled temperature field of an 80 kW MPMSM. When the motor operates at a rated speed of 27 r/min, the temperature distribution of each part in the motor is shown in Fig. 8. The cooling water velocity and waterway pressure distribution in the frame are shown in Fig. 9.

Fig. 8 shows the highest temperature of the stator tooth is 329.8 K. The highest temperature of the lower end of the stator winding is 351.8 K. The highest temperature of the rotor upper surface is 351.2 K. The highest temperature of the permanent magnet is 352.7 K. The maximum temperature rise of the winding is 51.8 °C, which meets the temperature rise requirements of class F insulation. The modular waterway structure has good cooling effect. In the radial structure, the corresponding coil is removed at the module combination, so the heat generated by the winding is lower, and its temperature is lower. However, there is no electrical insulation in the module combination of the stator core, and there is the local hot spot, so the temperature of the stator module combination is higher than that of other positions. The rotor always rotates at the rated speed, the modular waterway structure has no effect on the temperature distribution on the radial circumference of the rotor.

Fig. 9 shows the maximum water velocity is 1.16 m/s. The maximum water pressure in the waterway is 3.6 kPa, which meets the pressure requirements. When some module units in the MPMSM run over load, the water velocity can be increased to reduce the temperature rise, so that the motor can be fault-tolerant operation.

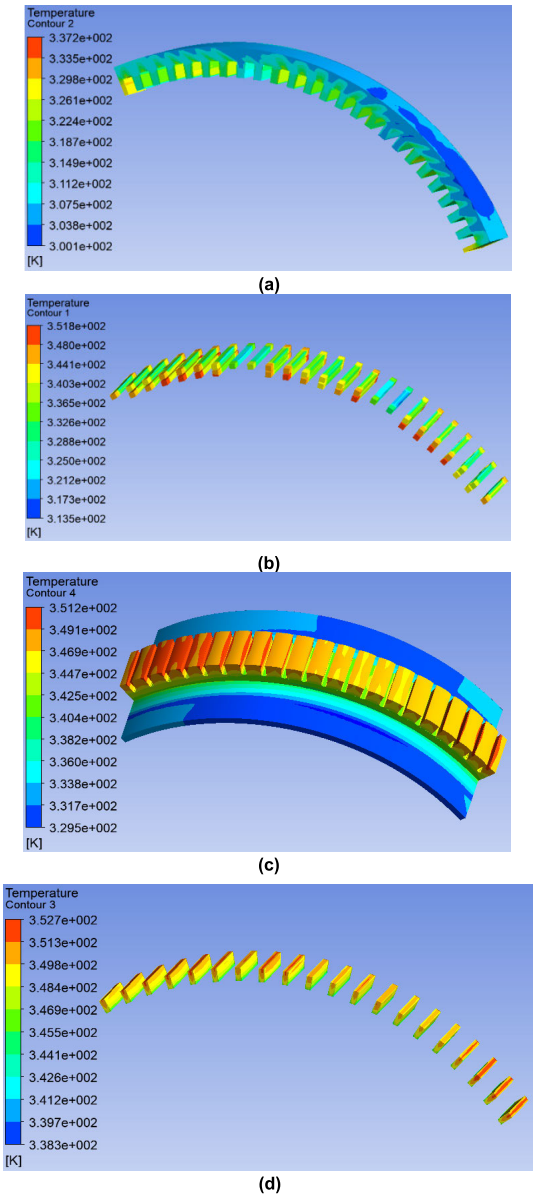

FIGURE 8. Temperature distribution: (a) stator; (b) winding; (c) rotor magnetic pole and sleeve; (d) permanent magnet.

V. PROTOTYPE DEVELOPMENT

To validate the rationality of the proposed calculation method for the modular waterway structure and temperature rise of MPMSM, an 80 kW prototype is developed, and its main parameters are shown in Table 3. The designed modular waterway structure is shown in Fig. 10.

When the prototype is running under the rated condition, we make the temperature rise experiment of the prototype and test the cooling effect of the designed modular waterway structure. The experiment platform is built, as shown in Fig. 11. It is composed of a ball mill, an 80 kW prototype, a controller of prototype, a belt conveyor, a torque sensor, a reducer, a induction motor and its frequency converter. The induction motor provides rated load for the ball mill through the belt conveyor, and the prototype is powered by

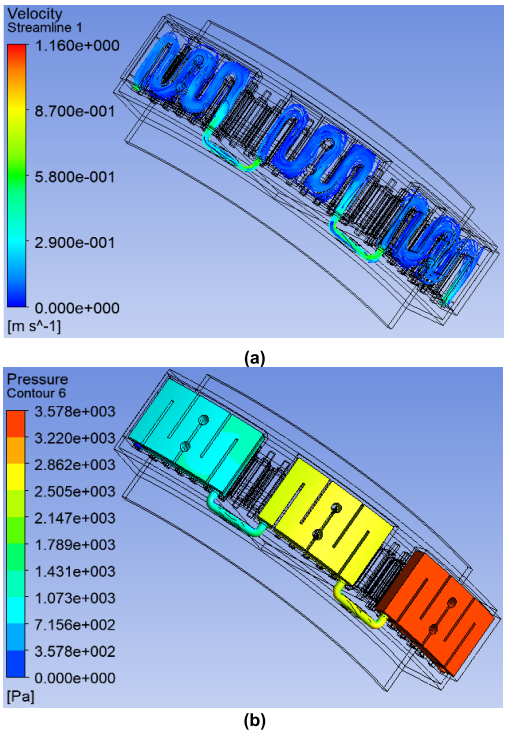

FIGURE 9. Water velocity and waterway pressure distributions in frame: (a) water velocity; (b) pressure.

TABLE 3. Main parameters of the MPMSM.

Items	Value
Rated power (kW)	80
Rated voltage (V)	380
Rated current (A)	135
Rated frequency (Hz)	18
Rated speed (r/min)	27
Rated torque (N·m)	22310
Stator outer diameter (mm)	2200
Stator inner diameter (mm)	2000
Core length (mm)	185
Rotor outer diameter (mm)	1995.6
Rotor inner diameter (mm)	1876.6
Pressure limitation of inlet and outlet (kPa)	30

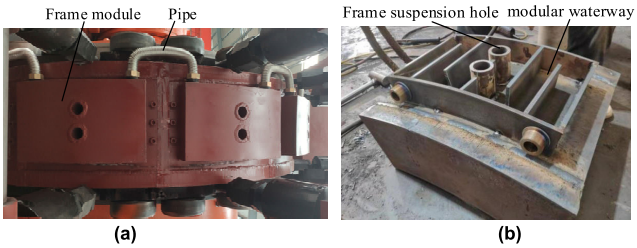

FIGURE 10. Modular frame of prototype: (a) frame; (b) cooling channel.

the controller to drive the ball mill to run. The temperature rise experiment is carried out under the cooling water flow of 1.5 m^3/h. After 90 minutes, the temperature rise of the MPMSM reached a stable level, as shown in Fig. 12. The stable temperatures of the winding is 79.8 °C, which meets the requirements of class F insulation. The frame temperature is 32.2 °C. The motor inlet temperature is 21.2 °C, the

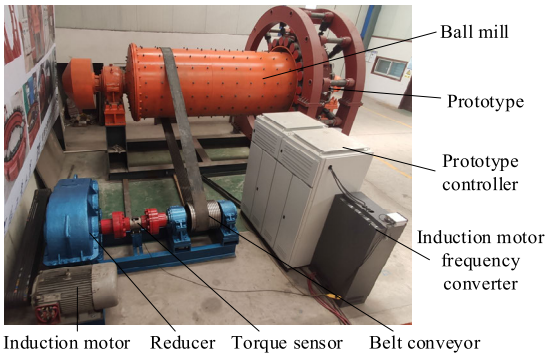

FIGURE 11. Prototype experiment platform.

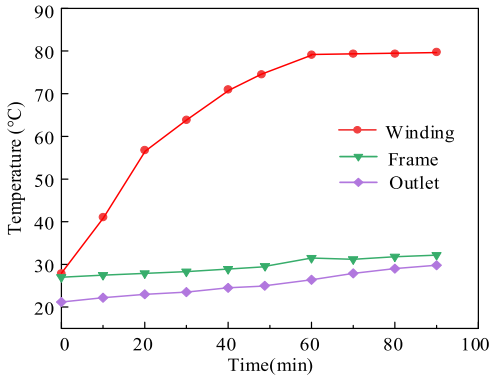

FIGURE 12. Temperature curves of prototype.

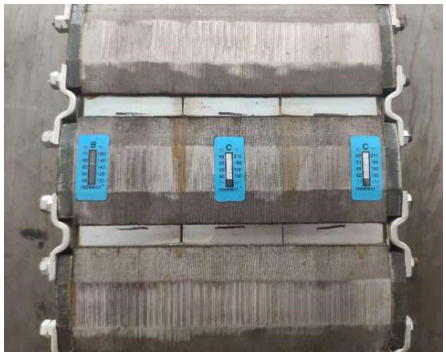

FIGURE 13. Prototype rotor temperature.

outlet temperature is 29.8 °C, and the temperature difference between the two is 8.6 °C. The temperature distribution of the rotor is shown in Fig. 13. The temperatures at the end and middle of the rotor are 77.5 °C and 77 °C, respectively.

The temperatures of MPMSM components calculated by the 3D equivalent thermal network method (ETNM), the fluid-solid coupled finite element method (FCFEM), and the experiment values and calculation errors are listed in Table 4. The calculation results of 3D ETNM and FCFEM are basically the same as the experiment results, and the errors of two methods are within a reasonable range of calculation errors. The experiment results show that the modular waterway structure based on 3D ETNM has good cooling effect and meets the temperature rise requirements of large MPMSM.

TABLE 4. Comparison between calculation and experiment results.

Components	ETNM (°C)	FCFEM (°C)	Experiment (°C)	ETNM error (%)	FCFEM error (%)
Frame	30.2	31.2	32.2	6.2	3.1
Winding	79.6	77.3	79.8	0.3	3.1
Magnet	80.8	79.4	—	—	—
Rotor pole	79.4	77.6	77.3	2.7	0.6
Stator core	47.7	46.1	47.5	0.4	2.9
Rotor sleeve	71.7	67.8	—	—	—
End cover	38.0	36.9	—	—	—
Bearing	58.0	—	—	—	—

VI. CONCLUSION

This paper proposes a 3D equivalent thermal network method to study the cooling problem of MPMSM. The modular waterway design process of the motor is discussed, and its cooling effect is analyzed. The following conclusions are drawn.

(1) According to the modular structure, a 3D equivalent thermal network model is established to calculate the temperature distributions of the axial nodes of the whole motor and the radial nodes of a sub-module.

(2) The modular waterway structure is designed based on a 3D equivalent thermal network method. The fluid-solid coupled temperature field is simulated for the axial series modular waterway structure, and its cooling effect is good.

(3) An 80 kW prototype is made, its experiment results verifies that the designed modular waterway structure meets the requirements of temperature rise. At the same time, the correctness of the designed modular waterway structure based on a 3D equivalent thermal network method is verified, which provides a reference for the research on the cooling problem of MPMSM.

ACKNOWLEDGMENT

Thanks to Tiantian Liang for providing guidance on the article, Mingxia Xu for proof reading the article. Thanks to Chuanfang Xu and Qingguang Chi for the data processing and writing assistance and Haiyu Liu for the language help. Many thanks for their kind help during the research.

REFERENCES

[1] G. J. Li, Z. Q. Zhu, W. Q. Chu, M. P. Foster, and D. A. Stone, "Influence of flux gaps on electromagnetic performance of novel modular PM machines," *IEEE Trans. Energy Convers.*, vol. 29, no. 3, pp. 716–726, Sep. 2014.

[2] Y. X. Li, Z. Q. Zhu, A. S. Thomas, Z. Y. Wu, and X. M. Wu, "Novel modular fractional slot permanent magnet machines with redundant teeth," *IEEE Trans. Magn.*, vol. 55, no. 9, pp. 1–10, Sep. 2019.

[3] X. Fan, D. Li, R. Qu, C. Wang, and H. Fang, "Water cold plates for efficient cooling: Verified on a permanent-magnet machine with concentrated winding," *IEEE Trans. Ind. Electron.*, vol. 67, no. 7, pp. 5325–5336, Jul. 2020.

[4] L. Li and G. Zhu, "Electromagnetic-thermal-stress efforts of stator-casing grease buffers for permanent magnet driving motors," *IEEE Trans. Ind. Appl.*, early access, pp. 1–9, Jul. 2023, doi: 10.1109/TIA.2023.3291680.

[5] G. Zhu, Y. Zhu, W. Tong, X. Han, and J. Zhu, "Double-circulatory thermal analyses of a water-cooled permanent magnet motor based on a modified model," *IEEE Trans. Magn.*, vol. 54, no. 3, pp. 1–4, Mar. 2018.

[6] H. Vansompel and P. Sergeant, "Extended end-winding cooling insert for high power density electric machines with concentrated windings," *IEEE Trans. Energy Convers.*, vol. 35, no. 2, pp. 948–955, Jun. 2020.
[7] G. Du, W. Xu, J. Zhu, and N. Huang, "Power loss and thermal analysis for high-power high-speed permanent magnet machines," *IEEE Trans. Ind. Electron.*, vol. 67, no. 4, pp. 2722–2733, Apr. 2020.
[8] T. A. Huynh and M.-F. Hsieh, "Improvement of traction motor performance for electric vehicles using conductors with insulation of high thermal conductivity considering cooling methods," *IEEE Trans. Magn.*, vol. 57, no. 2, pp. 1–5, Feb. 2021.
[9] X. Y. Wang, S. S. Liu, L. X. Wang, and P. Gao, "Impact of the motor length-to-diameter ratio on the selection of cooling water channels for the permanent magnet synchronous motor," *IEEJ Trans. Elect. Electron. Eng.*, vol. 18, no. 11, pp. 1815–1825, Aug. 2023.
[10] W. F. Yu, W. Hua, J. Qi, H. L. Zhang, G. Zhang, H. F. Xiao, S. Xu, and G. T. Ma, "Coupled magnetic field-thermal network analysis of modular-spoke-type permanent-magnet machine for electric motorcycle," *IEEE Trans. Energy Convers.*, vol. 36, no. 1, pp. 120–130, Mar. 2021.
[11] D. Liang, Z. Q. Zhu, B. Shao, J. Feng, S. Guo, Y. Li, and A. Zhao, "Estimation of two- and three-dimensional spatial magnet temperature distributions for interior PMSMs based on hybrid analytical and lumped-parameter thermal model," *IEEE Trans. Energy Convers.*, vol. 37, no. 3, pp. 2175–2189, Sep. 2022.
[12] H. Liange, C. Hongling, and S. Wenjun, "Boiling heat transfer-based temperature rise characteristics of automotive permanent magnet synchronous motors at peak operating conditions," *J. Mech. Sci. Technol.*, vol. 36, no. 7, pp. 3691–3699, Jul. 2022.
[13] R. Lehmann, M. Künzler, M. Moullion, and F. Gauterin, "Comparison of commonly used cooling concepts for electrical machines in automotive applications," *Machines*, vol. 10, no. 6, p. 442, Jun. 2022.
[14] Z. Hao, J. Shuanbao, W. Dong, W. Gongbao, and H. Pengfei, "Design and analysis of the integrated motor cooling system for shaftless propeller," *IEEE Access*, vol. 7, pp. 174573–174582, 2019.
[15] Y. Shi, J. Wang, and B. Wang, "Electromagnetic-thermal coupled simulation under various fault conditions of a triple redundant 9-phase PMASynRM," *IEEE Trans. Ind. Appl.*, vol. 56, no. 1, pp. 128–137, Jan. 2020.
[16] Y. Tang, L. Chen, F. Chai, and T. Chen, "Thermal modeling and analysis of active and end windings of enclosed permanent-magnet synchronous in-wheel motor based on multi-block method," *IEEE Trans. Energy Convers.*, vol. 35, no. 1, pp. 85–94, Mar. 2020.
[17] Y. Xu, B. Zhang, and G. Feng, "Electromagnetic design and thermal analysis of module combined permanent magnet motor with wrapped type for mine ball mill," *IET Electric Power Appl.*, vol. 16, no. 2, pp. 139–157, Feb. 2022.
[18] Y. Xu, B. Zhang, and G. Feng, "Research on thermal capacity of a high-torque-density direct drive permanent magnet synchronous machine based on a temperature cycling module," *IEEE Access*, vol. 8, pp. 155721–155731, 2020.
[19] M. Polikarpova, P. Ponomarev, P. Röyttä, S. Semken, Y. Alexandrova, and J. Pyrhönen, "Direct liquid cooling for an outer-rotor direct-drive permanent-magnet synchronous generator for wind farm applications," *IET Electric Power Appl.*, vol. 9, no. 8, pp. 523–532, Sep. 2015.
[20] X. Jiang, Y. Zhang, S. Jin, F. Zhang, and C. Gerada, "A novel thermal network model used for temperature calculation and analysis on brushless doubly-fed generator with winding encapsulating structure," *IEEE Trans. Ind. Appl.*, vol. 55, no. 2, pp. 1473–1483, Mar. 2019.

YINGYING XU was born in Wafangdian, Liaoning, China, in 1992. She received the B.S., M.S., and Ph.D. degrees in electrical engineering from the Shenyang University of Technology, Shenyang, China, in 2016, 2018, and 2022, respectively. She is currently a Postdoctoral Researcher of electrical engineering with Tianjin University, Tianjin, China. She is also a Lecturer with the School of Automation and Electrical Engineering, Dalian Jiaotong University, Dalian, China. Her research interests include the design and control of special motors, low-speed high-torque drive systems, and permanent magnet direct drive technology.

TIANTIAN LIANG was born in Nehe Heilongjiang, China, in 1986. He received the B.S. degree in automation from the Harbin University of Science and Technology, in 2009, the M.S. degree in detection technology and automatic equipment from Harbin Engineering University, in 2012, and the Ph.D. degree in mechanical engineering in control science and engineering from the Harbin Institute of Technology, in 2019. He is currently a Lecturer with the School of Automation and Electrical Engineering, Dalian Jiaotong University, Dalian, China. His research interests include the fault diagnosis of traction motors, intelligent fault diagnosis, and fault tolerant control of high-speed trains.

MINGXIA XU was born in Wenzhou, Zhejiang, China, in 1985. He received the M.S. degree in theory and new technology of electrical engineering from Zhejiang University, in 2012, and the Ph.D. degree in theory and new technology of electrical engineering from the Dalian University of Technology, in 2022. He is currently an Associate Professor with the School of Automation and Electrical Engineering, Dalian Jiaotong University, Dalian, China. His current research interests include the auxiliary converters for urban rail transit and control of the metro traction drive systems.

CHUANFANG XU was born in Linyi, Liaoning, China, in 1978. She received the B.S. and M.S. degrees in electrical engineering and traffic information engineering and control from Dalian Jiaotong University, Dalian, China, in 2001 and 2006, respectively, and the Ph.D. degree in power electronics and power transmission from the Dalian University of Technology, Dalian, in 2020. She is currently an Associate Professor with the School of Automation and Electrical Engineering, Dalian Jiaotong University. Her current research interests include motor drive and control, operation control, and adhesion control of high-speed trains.

QINGGUANG CHI was born in Wafangdian, Liaoning, China, in 1985. He received the B.S., M.S., and Ph.D. degrees in electrical engineering from the Shenyang University of Technology, Shenyang, China, in 2008, 2011, and 2020, respectively. He is currently an Associate Professor with the School of Automation and Electrical Engineering, Dalian Jiaotong University, Dalian, China. His research interests include the design and control of special motors, low-speed high-torque drive systems, permanent magnet direct drive technology, and vibration and noise of high-frequency transformers.

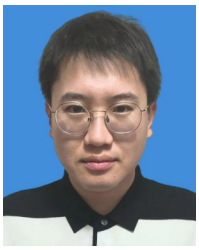

HAIYU LIU was born in Wafangdian, Liaoning, China, in 1994. He received the B.S. degree in electrical engineering and automation from the Shenyang University of Technology, Shenyang, China, in 2016. He is currently an Engineer with CRRC Dalian Company Ltd., Dalian, China. His research interests include the design and control of special motors.